

# **Cuda Implementation of Advanced Pencil Sketch Filter**

Andreas Altergott, Raphael Braun, Stefan Burnicki

August 26, 2014



# Cuda Implementation of Advanced Pencil Sketch Filter

Andreas Altergott, Raphael Braun, Stefan Burnicki

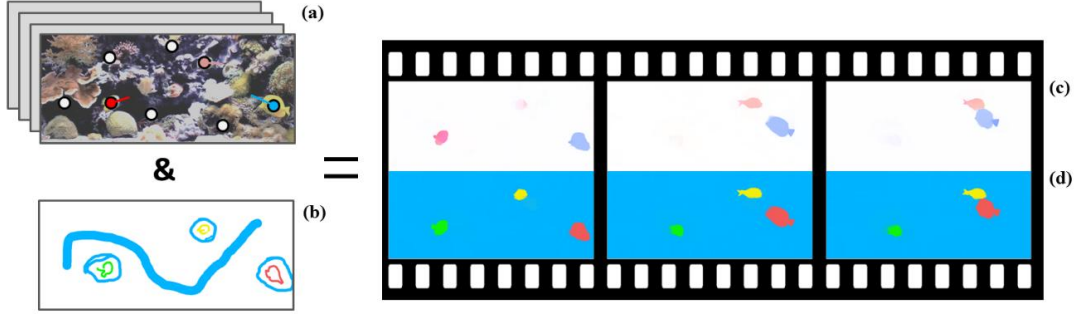


Figure 1: A application of the presented method is to consistently propagate user input scribbles through a video. Optical flow (c) is calculated from the input video (a) using sparse feature matching. Then the scribbles (b) are spread in space and time to generate (d)

## Abstract

This report is about blabla.

## 1 Introduction

Creating pencil sketches have a very long history. Throughout time artist have perfected the art of creating pencil drawings in all thinkable styles, ranging from completely abstract to stunningly photorealistic. However such skills are rare, and only well trained artists or passionated hobby artists are able to actually create pleasing looking images using nothing but the eye, a paper and a pencil. Today, in a time where cameras can be used to capture a realworld scene in a matter of seconds, with accurate proportions and colors and no skills, the need for pencil sketches seem to be gone. However, photographs do not convey the same emotions that sketches do. There is a certain timeless flair to pencil sketches that makes them just nice to look at.

Therefore designing an pencil sketch filter, which produces a pencil sketch from a regular photograph is an exciting task. The filter described in [LXJ12] is such a filter, which consists of two stages: sketching the outlines and drawing the shading. In the sketch stage the filter calculates several line convo-

lutions and the shading stage solves a huge linear system of equations. Both tasks are computationally rather expensive and according to the authors their implementation of the filter takes 2 seconds to run on a  $600 \times 600$  image.

This report presents our efforts to implement the entire filter on the GPU using Cuda. The structure is as follows: The filter itself is described in Section 3, then in Section 4 we describe our implementation using Cuda. Section 5 shows our benchmarking results for various input images and Section 6 some possible optimizations and applications for our implementation.

## 2 Previous Work

Use this (a completely different very cool scetch filter on the GPU) [LSF10] and this (3d Models => Scetch): [BLC<sup>+</sup>12]

## 3 Method

The problem class that is addressed by the paper can be solved by minimizing error functions in the form:

$$E(J) = E_{data}(J) + \lambda E_{smooth}(J) \quad (1)$$

Where  $J$  is the unknown solution,  $E_{data}$  the application specific error term and  $E_{smooth}$  the regular-

ization term which enforces neighborhood smoothness.

Instead of solving this expensive optimization all at once, the data term is calculated locally ( $E(J) = E_{data}(J)$ ). The regularization term is replaced by a edge aware filtering operation, which is then applied on  $J$ . This means smoothness is created instead of solved for with a optimization.

To understand the mathematical justification for replacing a global optimization by a local smoothing operation the method is explained for the calculation of one single optical flow image as an example.

Given two consecutive images in a video  $I_t$  and  $I_{t+1}$ , the pixel in the unknown optical flow image  $J(x, y)$  are motion vectors  $\vec{\omega}(x, y) = (u_{x,y}, v_{x,y})$  which describe the motion of pixel  $(x, y)$  from  $I_t$  to  $I_{t+1}$ . The data term for the optical flow estimation is:

$$E_{data}(u, v) = \sum_{(x,y)} ||I_t(x + u, y + v) - I_{t+1}(x, y)||^2 \quad (2)$$

This means the color differences between the start pixels and the pixels to which the motion vectors are pointing have to be as small as possible. The regularization term is given as:

$$E_{smooth}(u, v) = \sum_{(x,y)} (||\nabla u_{x,y}||^2 + ||\nabla v_{x,y}||^2) \quad (3)$$

$\nabla$  is the gradient magnitude operator, which measures the change of a value at one position of the video volume. Little variations results in small values (smooth), while big variations will create big values (noise). So  $E_{smooth}$  enforces smoothness to the flow by minimizes the total quadratic variance of the flow gradient.

By interpreting optical flow as a reaction-diffusion-system Equation 3 can be considered the Dirichlet's energy of  $\vec{\omega}$ . Minimizing it is equivalent to solving the Laplace equation  $-\Delta\vec{\omega} = 0$ . The data term can be added to this minimization as boundary condition. This yields a related heat equation, which is a special differential equation with some initial conditions:

$$\frac{\partial \vec{\omega}}{\partial t} = \alpha \Delta \vec{\omega} \quad (4)$$

$\vec{\omega}$  is initialized as Dirac function based on the data

term:

$$\vec{\omega} = \begin{cases} J(x, y) & \text{if } \exists (x, y) \in J \\ \vec{0} & \text{otherwise} \end{cases} \quad (5)$$

The function which is the solution to this differential equation is the function which has to be applied to  $J$  (from the data term) to solves our optical flow problem. In the isotropic case this function is known to be a Gaussian convolution. However, images form a inhomogeneous medium and the solution to the resulting nonlinear Partial Differential Equation is a anisotropic diffusion. Please refer to [Wei98] for details in using anisotropic diffusion for solving PDEs. [PKT09] showed that anisotropic diffusion is asymptotically equivalent to edge aware filtering, at least in the discrete setting, which is good enough, as images are represented discretely.

That is why the regularization in Equation 3 can be replaced by an edge-aware filtering on the correct input data  $J$ , which in the case of optical flow can be calculated from Equation 2. The initialization of  $J$  can be sparse as indicated in Equation 5. The authors of the presented paper exploit this feature to calculate the initialization only for SIFT and Lucas-Kanade features. It is very simple to find matches for such features in consecutive video frames which results in efficient and reliable initial flow estimations. The authors use an out of the box implementation from the openCV library for this. The only thing that is left to do for the one-frame optical flow example is to specify the used edge-aware filter.

**Domain Transform** The domain transform edge aware filter from [GO11] is used and later extended for temporal filtering. The edge awareness of a filter typically is based on filter weights which change based on the image content. The domain transform works differently. It transforms the distances between input pixels based on the image content, such that a simple Gaussian filter on the transformed image yields an edge aware result in the original domain. This transformation can only be done for 1D signals. However by applying the filter repeatedly to all rows (1D) and all columns (1D) a full 2D Image can be filtered. The filtered solution after  $N$  iterations is will be referred to as  $J'$ . Figure 2 illustrates the transformation and filtering process.

A joined domain-transform filtering is used, meaning the domain transform is calculated from the input image  $I$ . This transformation is then used

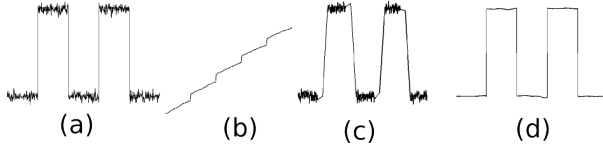


Figure 2: 1D domain transform example. (a) Input signal, (b) transform of the sample distances, (c) Transformed signal, (d) Result of filtering (c) with Gaussian filter and remap to original domain

to filter  $J$ . Thus edge informations are obtained directly from the image  $I$ , not from the flow estimate  $J$ .

The filter kernel (a sliding box filter) that is used in the domain transform filter step is no interpolation filter, which is a problem if  $J$  is sparsely initialized. Therefore the authors use a normalization image  $G$ . For pixels  $i$  in  $J$ , that were actually initialized, the corresponding pixel in  $G$  are set to one:  $G_i = 1$ . Pixels that do not contain data in  $J$  are set to 0.  $G$  is filtered with the exact same filter operation as  $J$ . The final result is computed as  $J'' = \frac{J'}{G'}$ . Figure 3 shows the result of this joint filtering operation on 1000 randomly chosen color values from a  $250 \times 250$  image.



Figure 3: Joint filtering. Left: Input image  $I$  for domain transform; Center: Sparse color input  $J$  generated by selecting 1000 random pixels from  $I$ , Right: Result of the joint filtering ( $J'' = \frac{J'}{G'}$ )

**Temporal Filtering** An additional filtering dimension is added to filter through time. As the domain transform filter is separable and is already performing an  $N$ -step iteration along  $X$  and  $Y$  direction, it is no problem to add another temporal dimension  $T$ . One filter iteration will therefore consist of three filtering passes: a pass in  $X$  direction, in  $Y$  direction and finally the result is filtered along the motion path of the pixel through the video volume ( $T$ ). An example for such a motion path is shown in

Figure 4. The pixels along the path are filtered just like a regular row or column. Those paths are generated by following the optical flow vectors in each frame, thus optical flow always has to be calculated for the filtering regardless of the final application.

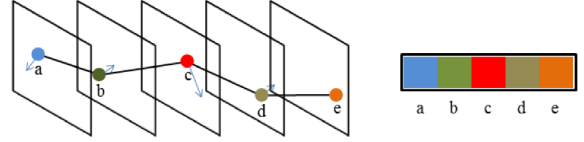


Figure 4: The motion path of one pixel. It is calculated by following the optical flow vectors (blue arrows). The temporal filter pass is applied to the resulting 1D color vector (a,b,c,d,e)

Requiring optical flow in order to calculate optical flow is a chicken egg problem, which is solved by iteratively improving a rough estimation of the flow. The first estimation is calculated using the sparse feature matching and one spacial joint filtering step in  $X$  and  $Y$  direction. This initial guess is then directly used for the first temporal pass  $T$ . The flow is then updated in each of the  $N$   $X$ - $Y$ - $T$  iteration steps.

Three special cases have to be considered when filtering along a motion path:

1. A path leaves the image boundaries
2. Multiple paths point to one pixel
3. No path from the previous frame is pointing to a pixel

Those cases are caught and handled such that each pixel in every frame belongs to exactly one path: All pixels that do not belong to a path (due to 1. or 3) are selected. New paths are created at the center of those pixels and initialized by filtering backwards in time. In case 1. the path is ended and the sliding box filter stops there. In case 2. one randomly chosen path is kept, while the others are ended in the previous frame.

The filter sizes for the spacial passes ( $\sigma_s, \sigma_r$ ) and for the temporal pass ( $\sigma_{st}, \sigma_{rt}$ ) can be controlled separately.

**Confidence** Thanks to the normalization image  $G$  it is very simple to add confidence values  $\beta_i$  to the initial data  $J_i$ , where  $i$  is a pixel in a frame.

Differences of matched feature descriptors can be used as confidence values for the optical flow and disparity estimation. The better the matches the higher the confidence. The confidence is directly written into the normalization image  $G_i = \beta_i$  and multiplied to the data image  $J$  by a per element multiplication  $J \cdot G$ . The result is then calculated the same way as before:  $J'' = \frac{(G \cdot J)'}{G'}$ . Figure 5 illustrates the effect of the confidence values.

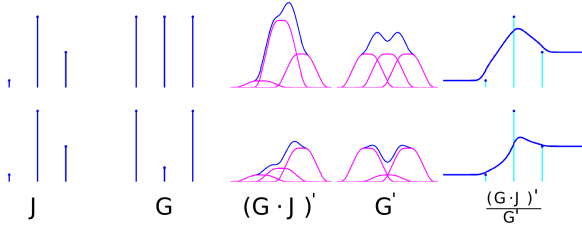


Figure 5: Demonstration of the confidence values applied to a 1D signal. In the top row all samples have the same confidence. In the bottom row the confidence of the middle sample is reduced. The purple line shows the contribution of a point.

**Iterative Occlusion Estimates** An occlusion estimate is added, which lowers the confidence in regions where the flow estimations prove to be unreliable. This automatically emphasizes reliable estimations. The reliability of a flow vector is estimated by computing both forward and backward flow vectors ( $\vec{\omega}^f$  and  $\vec{\omega}^b$ ) in each frame and applying a penalty function  $\rho$  to the sum of those vectors. As they point in different directions, their sum should be 0:

$$\rho = \left(1 - \left|\vec{\omega}^f + \vec{\omega}^b\right|\right)^\theta \quad (6)$$

$\theta$  defines the shape of the curve and was set to 5 for all applications (see Figure 6). The penalty has to be updated in each iteration as the flow changes. In the  $n$ th iteration  $G^n$  is updated with  $G^n = G^{n-1} \cdot p^{n-1}$ .  $J^n$  is updated the same way:  $J^n = J^{n-1} \cdot p^{n-1}$ .

### 3.1 Evaluation

Figure 7 shows the improvements that are gained by the described methods. The first two rows are optical flow vectors and the last a scribble propagation. The first column shows the result when the temporal dimension is naively filtered straight

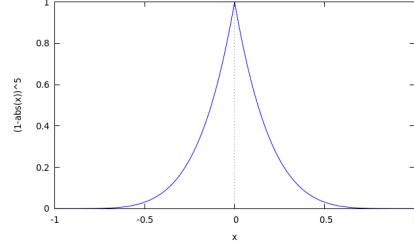


Figure 6: Shape of the penalty function for  $\theta = 5$ .

through the video volume. For the second volume motion paths were followed. The last two columns show the effect of confidence and occlusion estimation. Note that especially the edge regions are improved.

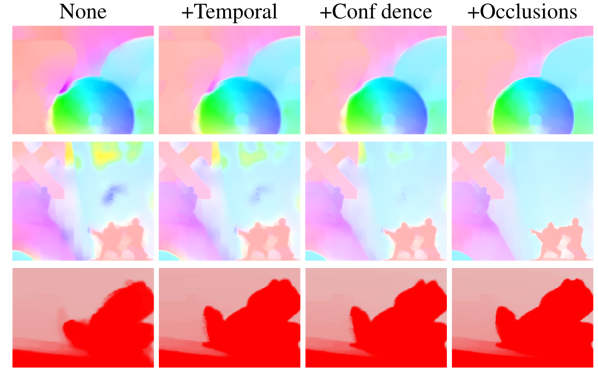


Figure 7: The effect of each processing step: temporal filtering, confidence and iterative occlusion estimates. The first two rows show color coded optical flow vector estimations, the last row is a scribble propagation which dyes a frog to be red.

There is no ground truth data available for long temporal optical flow computations, therefore a qualitative validation is not really possible. However the comparisons in the supplemental video to other state of the art methods suggest that this new method is superior to all other methods in respect to correctness and consistency.

The fact that a descriptor based feature matcher is used for the initial sparse optical flow calculation enables this method to correctly track small, fast moving object, as long as they have matchable features. Other optical flow calculation approaches use windows to reduce computation cost and scale-space pyramids for large motions, so fast

moving objects are detected in downscaled images. Therefore small fast moving objects disappear completely.

Table 1 shows a performance comparison of the presented approach to some state of the art optical flow calculation approaches.

Method	Time per output frame	Total for 8 frames
[RHB <sup>+</sup> 11]	55 seconds	7.3 minutes
[ZBW11]	620 seconds	1.4 hours
[VBVZ11]	40 minutes	5.4 hours
presented	625 ms	5 seconds

Table 1: Performance comparison for the optical flow calculation to different approaches on the same 8 frame sequence ( $640 \times 640$  resolution)

#### 4 GPU Implementation

The temporal consistency that can be achieved using the described method is usable for many applications, however as the optical flow is always needed for temporal filtering it is calculated no matter which application is implemented. Optical flow by itself can be used for various applications like frame interpolation, motion blur or motion magnification [LTF<sup>+</sup>05].

**Disparity Estimation** Disparity estimation is about computing the correspondence between a pair of stereoscopic images. The result  $J_{xy} = d_{xy}$  can be used as depth map for various tasks. Finding correspondences in stereoscopic images is very similar to calculating optical flow from consecutive video frames:

$$E_{data}(d) = \sum_{(x,y)} ||I^r(x + d_{xy}, y) - I^l(x, y)||^2$$

$$E_{smooth}(d) = \sum_{(x,y)} (||\nabla d_{xy}||)^2$$

$J$  is sparsely initialized by feature matches between  $I^r$  and  $I^l$  and then filtered as it was done for optical flow. Figure 8 shows an example.

**Colorization and Scribble Propagation** The approach can be used to propagate user input (pen strokes) through a given video. The scribbles can have arbitrary meaning like color input for colorization or ids for object labeling. The input scribbles  $s_j$  from frame  $j$  are used to initialize  $J_j = s_j$ . Then the joint temporal smoothing is applied to create

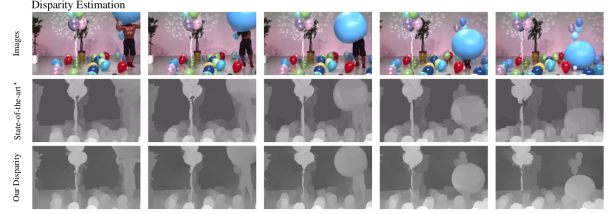


Figure 8: The results of the disparity estimation is compared of a state of the art dataset provided by the MPEG group for testing. Again the results of the proposed method is more stable in time. Less holes are randomly appearing and disappearing compared to MPEG data set.

intermediate frames. In average only every 20th frame needs own scribble data. Figure 1 shows an example for this application.

**Depth up-sampling** Depth sensor data from devices like Microsoft Kinects often suffer from bad resolution, temporal noise and holes. The authors use their technique to filter this data ( $J$ ) using the image data from the Kinects camera for the domain transform. As a result  $J'$  is getting up-sampled, holes are getting filled and noise is smoothed. Figure 9 shows a before-after comparison.

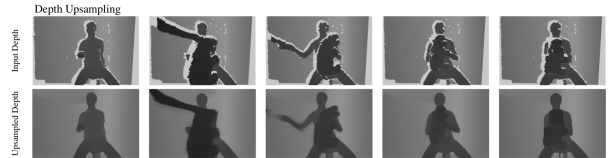


Figure 9: Low resolution and extremely noisy depth maps from a Microsoft Kinect is up-sampled and filled (white holes) using the same joint filtering operation as it is used for the optical flow calculation. The image data from the Kinect camera is used for the domain transform.

**Saliency** Visual saliency maps are used in many graphics applications as they highlight important regions in images. They can be used to change the aspect ratio of a video without distorting important features (persons). In this case temporal inconsistencies show up as wobbling. The authors used a per frame saliency calculation  $l$  as initialization for  $J(x, y) = l(x, y)$  and applied the temporal smoothness operation to gain consistent results. Figure 10

shows the difference between the unfiltered and the filtered saliency.

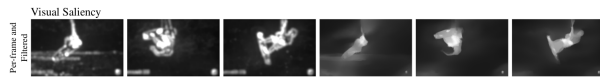


Figure 10: First three images show the per frame saliency calculation, which are then temporally filtered to create the smooth results on the right.

## 5 Performance

TODO

## 6 Future Work

TODO

## 7 Conclusion

A simple and efficient approach was presented that simplifies difficult global optimization problems like optical flow and disparity calculations using temporal edge aware filtering. The method creates temporal consistent results for many image based graphics problems. Sparse feature matches can be used as input for the joint filtering operation to replace costly global minimizations.

There are some limitations to the approach. It is possible that objects are not detected if they do not provide enough features to match. This issue can be addressed by adapting the parameters of the feature matcher to find as many features as possible. The effect of faulty features is minimal as their confidence is low, so they are filtered out.

As the method relies on edge preserving filtering problems occur if important object boundaries are not well defined in the input images. Unwanted bleeding artifacts can show up on such edges. Special care must be taken in the scribble propagation application to place the input scribbles close to edges, as object boundaries could otherwise be missed which causes unwanted color bleedings. A true global solution does not suffer from this problem. The authors suggested an extension that could fix this issue.

For me as writer of this report the described method in the paper was quite easy to comprehend and written in enough detail for a full reimplementation.

## References

- [BLC<sup>+</sup>12] Pierre B  nard, Jingwan Lu, Forrester Cole, Adam Finkelstein, and Jo  lle Thollot. Active Strokes: Coherent line stylization for animated 3D models. *NPAR 2012, Proceedings of the 10th International Symposium on Non-photorealistic Animation and Rendering*, June 2012.
- [GO11] Eduardo S. L. Gastal and Manuel M. Oliveira. Domain transform for edge-aware image and video processing. *ACM TOG*, 30(4):69:1–69:12, 2011. Proceedings of SIGGRAPH 2011.
- [LSF10] Jingwan Lu, Pedro V. Sander, and Adam Finkelstein. Interactive painterly stylization of images, videos and 3D animations. In *Proceedings of I3D 2010*, February 2010.
- [LTF<sup>+</sup>05] Ce Liu, Antonio Torralba, William T. Freeman, Fr  do Durand, and Edward H. Adelson. Motion magnification. *ACM Trans. Graph.*, 24(3):519–526, 2005.
- [LXJ12] Cewu Lu, Li Xu, and Jiaya Jia. Combining sketch and tone for pencil drawing production. In Paul Asente and Cindy Grimm, editors, *Expressive*, pages 65–73. ACM, 2012.
- [PKT09] S. Paris, P. Kornprobst, and J. Tumblin. *Bilateral Filtering: Theory and Applications*. Foundations and trends in computer graphics and vision. Now Publishers, 2009.
- [RHB<sup>+</sup>11] C. Rhemann, A. Hosni, M. Bleyer, C. Rother, and M. Gelautz. Fast cost-volume filtering for visual correspondence and beyond. In *Proceedings of the 2011 IEEE Conference on Computer Vision and Pattern Recognition, CVPR ’11*, pages 3017–3024, Washington, DC, USA, 2011. IEEE Computer Society.
- [VBVZ11] Sebastian Volz, Andr  s Bruhn, Levi Valgaerts, and Henning Zimmer. Modeling temporal coherence for optical



- flow. In Dimitris N. Metaxas, Long Quan, Alberto Sanfeliu, and Luc J. Van Gool, editors, *ICCV*, pages 1116–1123. IEEE, 2011.
- [Wei98] Joachim Weickert. *Anisotropic Diffusion in Image Processing*. ECMI Series. Teubner, Stuttgart, 1998.
- [ZBW11] Henning Zimmer, Andrés Bruhn, and Joachim Weickert. Optic flow in harmony. *Int. J. Comput. Vision*, 93(3):368–388, July 2011.